Graphene Oxide-BODIPY Conjugates as Highly Fluorescent Materials

Giacomo Reina, Giovanni Mariano Beneventi, Ramandeep Kaur, Giacomo Biagiotti, Alejandro Cadranel, Cécilia Ménard-Moyon, Yuta Nishina, Barbara Richichi, Dirk M. Guldi, Alberto Bianco

Graphene oxide-BODIPY conjugates as bright fluorescent material

Giacomo Reina,[#,&] Giovanni Mariano Beneventi,[#] Ramandeep Kaur,[#] Giacomo Biagiotti, Alejandro Cadranel, Cécilia Ménard-Moyon, Yuta Nishina, Barbara Richichi,* Dirk M. Guldi,* Alberto Bianco*

Giacomo Reina, Cécilia Ménard-Moyon, Alberto Bianco
CNRS, Immunology, Immunopathology and Therapeutic Chemistry, UPR 3572, University of Strasbourg, ISIS, 67000 Strasbourg, France
E-mail: a.bianco@ibmc-cnrs.unistra.fr

Giovanni Mariano Beneventi, Ramandeep Kaur, Alejandro Cadranel, Dirk M. Guldi
Department of Chemistry and Pharmacy & Interdisciplinary Center for Molecular Materials (ICMM), Friedrich-Alexander-Universität, Egerlandstrasse 3, 91058 Erlangen, Germany
E-mail: dirk.guldi@fau.de

Giacomo Biagiotti, Barbara Richichi
Department of Chemistry "Ugo Schiff", University of Firenze, Via della Lastruccia 13, 50019, Sesto Fiorentino, FI, Italy
E-mail: barbara.richichi@unifi.it

Yuta Nishina
Research Core for Interdisciplinary Sciences and Graduate School of Natural Science and Technology, Okayama University, 3-1-1 Tsushima-naka, kita-ku, Okayama 700-8530, Japan

[#]These authors contributed equally to this work.

[&]Current address: Empa Swiss Federal Laboratories for Materials Science and Technology Lerchenfeldstrasse 5, 9014 St. Gallen, Switzerland

Dedicated to the 70th birthday of Prof. Maurizio Prato

Keywords: Carbon nanomaterials, chemical functionalization, photoluminescent properties, transient absorption spectroscopy, imaging

Abstract

Covalent functionalization of graphene oxide (GO) with boron dipyrromethenes (BODIPYs) was achieved through a facile synthesis, affording two different GO-BODIPY conjugates where the main difference lies in the nature of the spacer and the type of bonds between the two components. The use of a long but flexible spacer afforded strong electronic GO-BODIPY interactions in the ground state. This drastically altered the light absorption of the BODIPY structure and impeded its selective excitation. In contrast, the utilisation of a short, but rigid spacer based on boronic esters resulted in a perpendicular geometry of the phenyl boronic acid BODIPY (PBA-BODIPY) with respect to the GO plane, which enables only minor electronic GO-BODIPY interactions in the ground state. In this case, selective excitation of PBA-BODIPY was easily achieved, allowing to investigate the excited state interactions. A quantitative ultrafast energy transfer from PBA-BODIPY to GO was observed. Furthermore, due to the reversible dynamic nature of the covalent GO-PBA-BODIPY linkage, some PBA-BODIPY is free in solution and, hence, not quenched from GO. This resulted in a weak, but detectable fluorescence from the PBA-BODIPY that will allow to exploit GO-PBA-BODIPY for slow release and imaging purposes.

1. Introduction

Ever since its isolation in 2004, graphene has tremendously attracted the attention for its potentials in the field of electronic materials.[1] In the last decade, we have seen the emergence of a full-fledged family of graphene-based materials (GBMs), which have been involved in a vast array of applications from polymer filler,[2,3] to sensing,[4–6] and energy storage.[7,8] In this context, graphene oxide (GO) has been by far the most studied carbon nanomaterial in the biomedical field.[9,10] GO and graphene share the same 2D "skeleton" structure. GO is composed of carbon, in which, however, about half of the C atoms are bound to different oxygen functionalities.[9,10] Such a characteristic is key in terms of forming stable GO colloids in water and/or in polar solvents. In contrast to graphene, GO is relatively easy to functionalize, owing to the varied functionalities, mainly epoxide and hydroxyl groups, on its surface.[11–13] Importantly, GO is rapidly degraded by human peroxidases avoiding long-term side effects that might be associated with bioaccumulation.[14]

In the fied of drug delivery, size and functionalization play an important role on how cells and tissues interact with materials.[15] GO is an excellent photoluminescence quencher, and as such it has been extensively used for biosensing. In this context, non-emissive GO-fluorophore adducts can be cleaved by specific conditions and, in turn, the photoluminescence of the fluorophore is reactivated.[16] A similar strategy has been also used for photodynamic therapy (PDT). In particular, when a photosensitizer is adsorbed onto GO, it is protected from photobleaching because fluorescence and the generation of reactive oxygen species (ROS) are inhibited. But, the photosensitizer becomes phototoxic after its release into the tumor cells.[17] Efficient photoluminescence quenching by GO renders GO-based materials, however, hard to be used for fluorescence bioimaging. Tracking GO is, nevertheless, essential to follow its fate in the body. Any residual activity of the fluorophores, which are in close proximity to GO, may be too weak for imaging. Different strategies have been pursued to tag GO with fluorescent dyes. One of them is based on supramolecular constructs of GO with small molecules bearing long or rigid spacers to prevent significant quenching.[18] We have recently reported the use of fluorescent GO-based platforms for *in vitro* and *in vivo* applications using biocompatible quantum dots.[19,20] In this context, a growing interest emerged to develop facile functionalization strategies with high yields, biocompatibility, and under mild conditions. Boron dipyrromethene (BODIPY) derivatives have been extensively studied for bioimaging and phototherapy.[21,22] BODIPYs show high singlet oxygen quantum yields, which make them ideal candidates for PDT[21,23] and phototermal therapy (PTT).[24,25] Moreover, their absorption

and fluorescence are adjustable by means of changing the substituents. BODIPYs have been successfully used in cancer therapy and diagnosis.[21] For example, BODIPYs have been exploited for PDT and combined to drug delivery, targeting, or fluorescence imaging applications.[21] Aza-BODIPYs stand also out for their strong absorption in the near infrared (NIR) range. The latter is a key condition for imaging and photosensitization.[23,26] Phenyl boronic acid BODIPY (PBA-BODIPY) has been grafted onto the catechol functions of reduced GO and employed for cancer cell imaging.[27] PEG-BODIPY (PEG, polyethylene glycol) has been employed for the non-covalent functionalization of GO. The resulting GO-PEG-BODIPY conjugates resulted promising for imaging, on one hand, and exploited as a photothermal and photodynamic platform *in vitro*, on the other hand.[28] In any of these cases, BODIPY have been isolated electronically from proximal GO by polymers, to avoid strong quenching of the BODIPY fluorescence. Quenching of BODIPY fluorescence, when adsorbed onto GO or reduced graphene oxide, has been attributed to charge transfer interactions that are driven by π-π interactions.[29] Interactions between GO and BODIPY have never been studied in detail in covalent conjugates. We recently reported the direct covalent functionalization to graft PBA-BODIPY by exploiting the diols present on the GO surface.[30] Our covalent approach permits an easy control on the BODIPY loading as we are forming stable conjugates. In particular, forming a boronic ester afforded a conjugate ready for imaging and photodynamic therapy. Understanding the interactions between GO and BODIPY in covalent architectures is absolutely necessary for preparing novel stable platforms in bioimaging and phototherapy.

In this work, we have prepared two different covalent conjugates between GO and PBA-BODIPY and studied their photophysical properties. To this end, two different approaches have been used for the functionalization of GO. An epoxide ring opening reaction afforded GO-NH-BODIPY with a long and flexible linker, while a boronic ester formation generated GO-PBA-BODIPY with a short but rigid linker. The two constructs show quite different steady-state and transient spectroscopic characteristics even if they are characterized by similar loading of BODIPY onto GO. Our results prompt to the importance of the spacer employed for the covalent functionalization of GO. A flexible and long spacer, as in the case of GO-NH-BODIPY, allows bending of the linker and π-π stacking of the chromophore onto the GO surface. Such interactions result in a broadening of the absorption and in a difficult selective light excitation. In strong contrast, in the case of GO-PBA-BODIPY, the absorption was far less affected by interactions with GO due to the rigid PBA spacer. The latter supports a nearly rigid perpendicular geometry of BODIPY with respect to the GO surface. The immediate consequence is the prevention of π-π stacking between BODIPY and GO. In this conformation,

ground state interactions between GO and BODIPY are minimal. Nevertheless, GO and BODIPY show strong interactions in the excited state. A quantitative energy transfer evolved from BODIPY to GO on a precedented time scale of less than 1 ps. Additionally, in agreement with the dynamic nature of the covalent linkage in GO-PBA-BODIPY, a little amount of fluorophore is free in solution and, hence, not quenched by GO. This behaviour results in a weak, but detectable fluorescence from the GO-PBA-BODIPY conjugate.

2. Results and discussions

2.1. Material functionalization and characterization

In this work, we have covalently conjugated two PBA-BODIPYs onto the surface of GO through two different chemical approaches. GO was produced by jet-milling with an average size of 430 nm.[30] The amino-functionalized PBA-BODIPY (called NH_2-BODIPY) was prepared by nucleophilic substitution of one of the chlorine atom of PBA-BODIPY using *N*-Boc-2,2′-(ethylenedioxy)diethylamine (Scheme S1, Figures S1-S6). The resultant mono-substituted BODIPY was then treated with trifluoroacetic acid to afford the deprotected NH_2-BODIPY. Subsequently, NH_2-BODIPY was grafted onto GO through the epoxide ring opening reaction (Scheme 1A). A second PBA-BODIPY was used to form boronic ester bonds with the diols present on the GO surface (Scheme 1B), as previously described.[30]

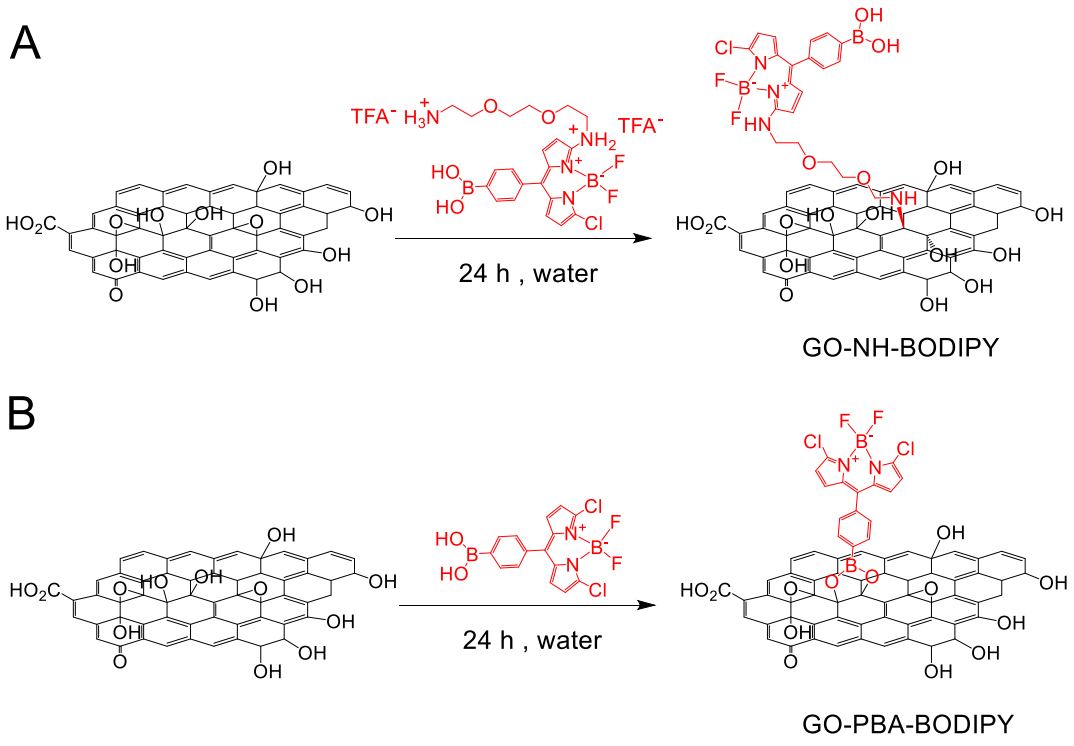

Scheme 1. Coupling of NH_2-BODIPY and PBA-BODIPY to GO through the epoxide ring opening reaction (A) and through the formation of a boronic ester (B) (each reaction is shown only on one functional group for clarity).

Both methodologies are versatile. They have been conducted in water and under mild conditions, which allows preserving the structure of GO. Subsequently, the crude products were purified through dialysis in water to yield the final conjugates, that is, GO-NH-BODIPY and GO-PBA-BODIPY. Due to possible side reactions of the boronic acid of NH_2-BODIPY with the diols on GO, the colorimetric Kaiser test was performed with GO-NH-BODIPY to assess the amount of free amines. Negative results indicated that the reaction between NH_2-BODIPY and GO involves selectively the epoxides and not the diols. GO was characterized before and after functionalization using different techniques, including FTIR (Figure S7), thermogravimetric analysis (TGA) performed in an inert atmosphere and X-ray photoelectron spectroscopy (XPS) (Figure 1).

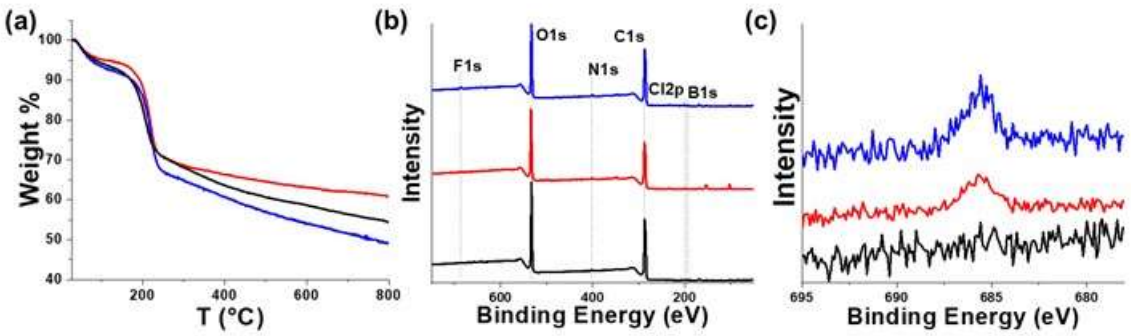

Figure 1. Characterization of GO (black line), GO-NH-BODIPY (red line), and GO-PBA-BODIPY (blue line): a) thermogravimetric analyses, b) XPS survey spectra, and c) F1s high resolution XPS spectra.

The thermal profile of GO (Figure 1a, black line) is best described by a three-step degradation. A first step, which is seen at around 100°C, relates to water desorption, a second one at 200°C corresponds to the degradation of labile oxygenated moieties, and a third one, conforming to a minor weight loss in the range above 250°C, is attributed to the removal of more stable oxygenated functional groups. Similar trends were observed for the functionalized materials. The thermal profile of GO-PBA-BODIPY shows another weight loss at about 200°C, which develops into a full degradation at 800°C. The latter is 6-7% larger than in pristine GO, confirming the successful conjugation reaction (Figure 1a, blue line). In the case of GO-NH-

BODIPY, the weight loss at 800°C is, however, 7-8% less compared to GO (Figure 1a, red line). A similar phenomenon was previously seen for GO functionalized with amines.[31–33] As GO is thermally unstable,[31,32] TGA is generally unsuitable for a precise estimation of GO functionalization loading.[11] Most importantly, the three main degradation steps of GO are maintained. This indicates that the functionalization did not affect the structural integrity of the material. In contrast, XPS is useful to assess the level of functionalization. XPS survey spectra of GO-PBA-BODIPY and GO-NH-BODIPY show the presence of B, Cl, N, and F around 190, 200, 400, and 685.6 eV, respectively (Figure 1b). Due to the high sensitivity of XPS, the %F has been taken into account for quantification,[34,35] and we have estimated a BODIPY loading of 110 and 200 μmol per gram of GO-NH-BODIPY and GO-PBA-BODIPY, respectively (Figure 1c). Overall, we have prepared and characterized two different GO-BODIPYs using two different spacers and covalent bonds.

2.2. Photophysical study

Following the preparation and characterization of the GO conjugates, we studied their photophysical properties and those of the precursors (Scheme 1). These characterizations are essential to understand and rationalize the interaction mechanism between GO and the fluorophores. Aqueous suspensions of GO feature characteristic absorptions in the UV region, which have been assigned to transitions arising from different domains (Figure 2). Absorptions at 231 nm are due to π-π^* transitions of C=C bonds as part of the sp^2-domains, while the absorptions at 303 nm relate to n-π* transitions of C=O bonds in the oxidized domains. The weak features in the visible region stem from band edge absorptions.[36]

In GO-PBA-BODIPY and GO-NH-BODIPY, in addition to the aforementioned GO absorptions, contributions from BODIPY-centred transitions are discernible at around 500 nm (Figure 2).[37] The BODIPY features are much more prominent in GO-PBA-BODIPY than in GO-NH-BODIPY, and this cannot be rationalized merely by the difference in BODIPY loading. An explanation is based on the different nature of the spacer in the two conjugates. Indeed, the comparison between the absorption of PBA-BODIPY and GO-PBA-BODIPY reveals that, after subtracting the GO-centred absorptions, PBA-BODIPY in its ground state is not strongly affected by the conjugation with GO (Figure 2a, inset). This observation is attributed to the phenylboronic ester that connects GO with BODIPY, which is likely to result in a rigid perpendicular arrangement of BODIPY with respect to the GO surface. Such conclusions are based both on the geometry of the diol defects in GO and the structure of the phenylboronic ester.[38–40] Such arrangement avoids strong electronic communications between them in the

ground state, in contrast to what is observed in the case of GO-NH-BODIPY. In the latter, the flexible spacer allows π-π stacking of BODIPY onto the GO surface, leading to broadened and red-shifted absorptions (Figure 2b). Notably, the BODIPY-centered absorption in GO-NH-BODIPY is so weak that a distinct absorption peak is only discernable after substracting the GO-centred absorptions (Figure 2b, inset).

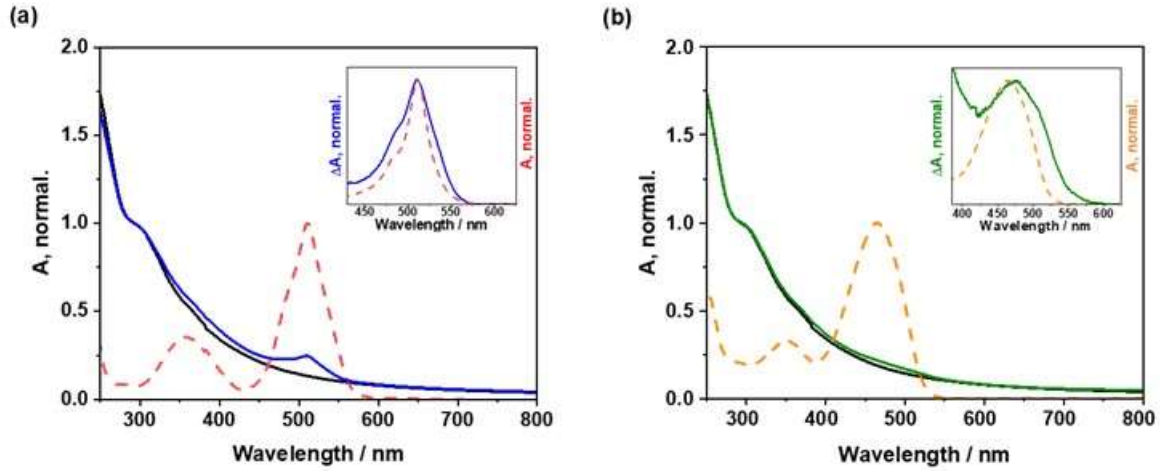

Figure 2. **(a)** Absorption spectra of GO (solid black line) and GO-PBA-BODIPY (solid blue line) normalized at 290 nm, and PBA-BODIPY (dashed red line) normalized at its absorption maximum. Inset: absorption spectrum of PBA-BODIPY (dashed red line) and absorption spectrum of GO-PBA-BODIPY (solid blue line) after the subtraction of the GO-centred absorption. **(b)** Absorption spectra of GO (solid black line) and GO-NH-BODIPY (solid green line) normalized at 290 nm, and NH_2-BODIPY (dashed orange line) normalized at its absorption maximum. Inset: absorption spectrum of NH_2-BODIPY (dashed orange line) and absorption spectrum of GO-NH-BODIPY (solid green line) after the subtraction of the GO-centred absorption.

In the excited state, GO is a well-known broad emitter. Its emission ranges from 500 to 900 nm and is excitation wavelength dependent (Figure 3a). The emisison originates from the recombination of electron–hole pairs in localized electronic states stemming from various possible configurations, in agreement with the strongly heterogeneous atomic and electronic structures of GO.[41] Such a broad emission is, however, similar to the tissue background rendering it poorly usable for bioimaging. Notably, the GO emission is seen when GO is photoexcited between 310 and 490 nm, but not at 500 nm and beyond. The fluorescence of PBA-BODIPY and NH_2-BODIPY is rather sharp and maximizes at 528 and 534 nm,

respectively (Figure 3b and 3c). The fluorescence quantum yield in water is 4.9% for PBA-BODIPY upon 480 nm photoexcitation and 4.3% for NH_2-BODIPY under 465 nm photoexcitation. 3D-fluorescence heat maps of GO-BA-BODIPY and GO-NH-BODIPY (Figures 3d and 3e) reveal contributions from both GO-centred and BODIPY-centred emissions. The latter features a 530 nm maximum in the case of GO-PBA-BODIPY and is far more intense than in the case of GO-NH-BODIPY, where the emission is barely detectable at 550 nm. All relevant photophysical properties are summarized in Table 1.This finding is well in line with the observations gathered by ground-state absorption spectroscopy. As such, the overall broadening of the NH_2-BODIPY absorptions when linked to GO renders its selective light excitation quite difficult.

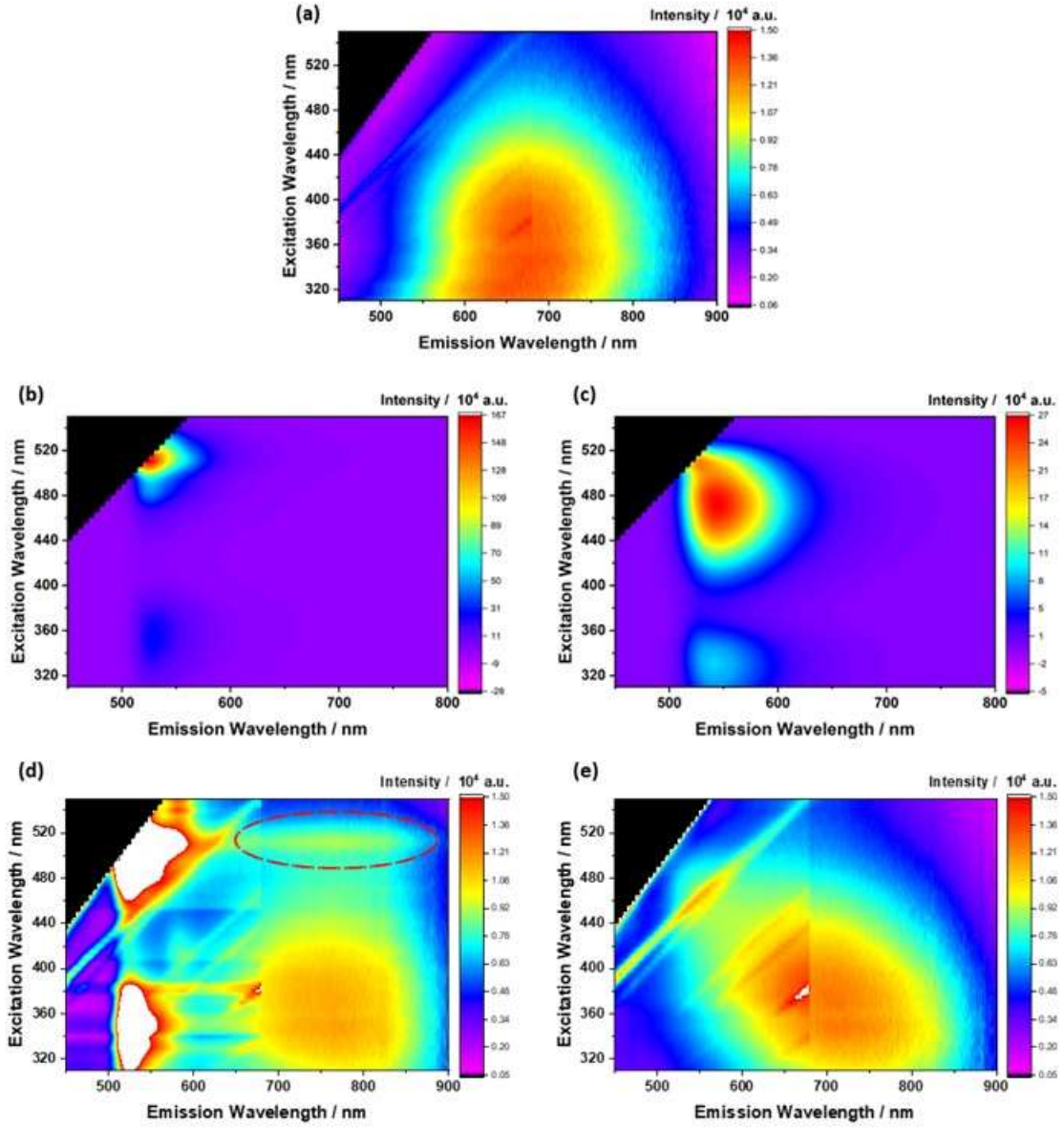

Figure 3. 3D-fluorescence heat maps of GO **(a)**, PBA-BODIPY **(b)**, NH_2-BODIPY **(c)**, GO-PBA-BODIPY **(d)**, and GO-NH-BODIPY **(e)** recorded in water under ambient conditions. The red dashed circle in (d) highlights the GO-centred emission originating from PBA-BODIPY energy transfer process. For GO and its conjugates a concentration of 10 mg/L was used, while for BODIPYs we used a 5×10^{-6} M concentration.

Table 1. Absorption and emission maxima, and emission quantum yields of the studied compounds in water.

	λ_{abs} (nm)	λ_{em} (nm)	QY_{em} (%)
GO	231, 303	680[b]	<0.01
PBA-BODIPY	358, 511	528	4.9
NH_2-BODIPY	351, 465	534	4.3
GO-PBA-BODIPY	231, 303, 511	528, 750[b]	0.16
GO-NH-BODIPY	231, 303, 478[a]	700[b]	<0.01

[a] Maximum associated to the weak BODIPY-centred absorption. [b] The GO emission band is broad and wavelength-dependent.

Transient absorption spectroscopy with GO-NH-BODIPY (Figure 5Sb), in which the NH_2-BODIPY-centred absorptions are not discernible, independently support this notion (*vide infra*). The aforementioned results help to exclude that the lack of BODIPY-centred fluorescence in the 3D-fluorescence heat map of GO-NH-BODIPY is merely due to a possible emission quenching by GO.[29] A closer look at the 3D-fluorescence heat maps revealed a difference in the intensity of the GO-centred emission in the two conjugates that is slightly more intense for GO-NH-BODIPY than for GO-PBA-BODIPY. Such differences are due to the inner filter effects at the excitation wavelength of BODIPY. This effect is surely more important in GO-PBA-BODIPY (Figure 2a). At this point, a quenching of the GO-centred emission as a result of functionalization cannot be excluded. In addition, an energy transfer from BODIPY to GO is observed for GO-PBA-BODIPY. This conclusion is based on the fact that GO-centred emission is observed upon photoexcitation at 510 nm (Figure 3d, red dashed circle), which corresponds to the absorption maximum of PBA-BODIPY. Notably, the BODIPY-centred fluorescence in GO-PBA-BODIPY has the exact same shape than seen for PBA-BODIPY in water (Figure S8a). We consider this result as a first indication of the presence of free PBA-BODIPY in GO-PBA-BODIPY suspensions. In the case of GO-NH-BODIPY, only the GO-

centered emission is observable while no distinct BODIPY-centered fluorescence is noted (Figure S8b). As such, free NH-BODIPY is absent in GO-NH-BODIPY.

Then, time-correlated single photon counting (TCSPC) experiments in water were performed by monitoring the fluorescence at 520 nm upon 355 nm photoexcitation (Figure S9). Fluorescence decays from PBA-BODIPY and GO-BA-BODIPY were both fitted with biexponential functions. For PBA-BODIPY two lifetimes, corresponding to 2.64 ns (94%) and 0.78 ns (6%) were derived. The long lifetime is assigned to the PBA-BODIPY singlet-excited state, while the short one relates to aggregated PBA-BODIPY, which is due to its poor solubility in water. The two lifetimes for GO-BA-BODIPY were 2.79 ns (94%) and 0.65 ns (6%), respectively. In this case, the long lifetime relates likewise to the PBA-BODIPY singlet-excited state. By virtue of the excellent match with those lifetimes seen in the references BODIPY-centred fluorescence, we postulate the presence of equilibrated free PBA-BODIPY in GO-PBA-BODIPY solutions. A reasonable explanation for this might be the dynamic nature of the reversible boronic ester bonds between GO and PBA-BODIPY.[42–44] As a matter of fact, in the case of GO-NH-BODIPY, where the linker is a non-dynamic covalent bond, no emission from free NH_2-BODIPY is observed. The short lifetime of GO-BA-BODIPY might stem from either aggregated free PBA-BODIPY or GO-centred emission, which has also a similar lifetime.[45] Notably, the absence of additional fluorescent features for GO-PBA-BODIPY (Figure S8a) suggests that the PBA-BODIPY-centred excited states are quantitatively quenched in the GO conjugate. A likely rationale is an energy transfer as observed in the steady-state experiments. To this end, considering the BODIPY-centred fluorescence quenching in GO-PBA-BODIPY (Figure S10) and after correcting for the inner filter effects, the percentage of free PBA-BODIPY was estimated to be around 3%.

Unambiguous proof for excited state interactions in GO-PBA-BODIPY came from transient absorption measurements. In particular, transient absorption spectra were recorded first for the GO, PBA-BODIPY, and NH_2-BODIPY followed by GO-PBA-BODIPY and GO-NH-BODIPY. For all of them, 500 nm photoexcitation was employed. Starting with GO (Figure 4a) we note ground state bleaching signals from 420 to 550 nm, which are attributed to quantum-confined graphene-like states.[46] Excited-state absorptions were observed across the spectral range from 550 to 1300 nm, which are attributed to directly excited oxygen-containing functionalities.[46] We employed a three-species sequential kinetic model to fit the raw data and from the corresponding global analysis we derived species associated spectra (SAS) with lifetimes of 6 ps, 83 ps, and 6.9 ns for SAS1, SAS2, and SAS3, respectively. The shortest lifetime stems from electron-(acoustic) phonon interactions,[47,48] while the remaining two

should originate from the slow de-trapping of electrons located in traps of different depths.[48,49] The lifetime due to electron-(acoustic) phonon interactions is consistent with the literature reports.[48] In contrast, the kinetics of de-trapping are slower than those reported in the literature: we observed 83 ps rather than 39 ps and 6.9 ns rather than 205 ps. Their nature depends primarily on the trap density in the GO sample.[49,50] As such, variations in terms of lifetimes are not surprising. Notably, the spectroscopic features of the three species lack any appreciable differences. Next, the transient absorption measurements for PBA-BODIPY (Figure 4b) and NH_2-BODIPY (Figure S12a) revealed bleaching of the ground-state absorptions along with stimulated emission in the range from 510 to 560 nm. Prominent singlet-excited state features evolve at 450-490 nm together with a weak transient beyond 600 nm. In the case of PBA-BODIPY, its poor solubility in water limits its investigation to solvent mixtures. Global analysis based on a three-species sequential kinetic model was employed for the fitting, which resulted in lifetimes of 2.8 ps, 109 ps, and 2.0 ns, respectively. The short lifetime relates to solvent reorganization and vibrational relaxations of the initially formed singlet-excited state, while the long lifetime corresponds to the decay of the relaxed singlet-excited state. The intermediate lifetime is associated with the deactivation of aggregated PBA-BODIPY species in solution. This finding is consistent with TCSPC measurements both in water and in the solvent mixture (Figure S11). When turning to NH_2-BODIPY, global analysis was based on a three-species sequential kinetic model as well. The 2 ps lifetime reflects the energy dissipation in the form of solvent and vibrational relaxations. The 72 and 680 ps lifetimes are ascribed to the deactivation of the relaxed singlet-excited states of either aggregates and or monomers of NH_2-BODIPY, respectively.

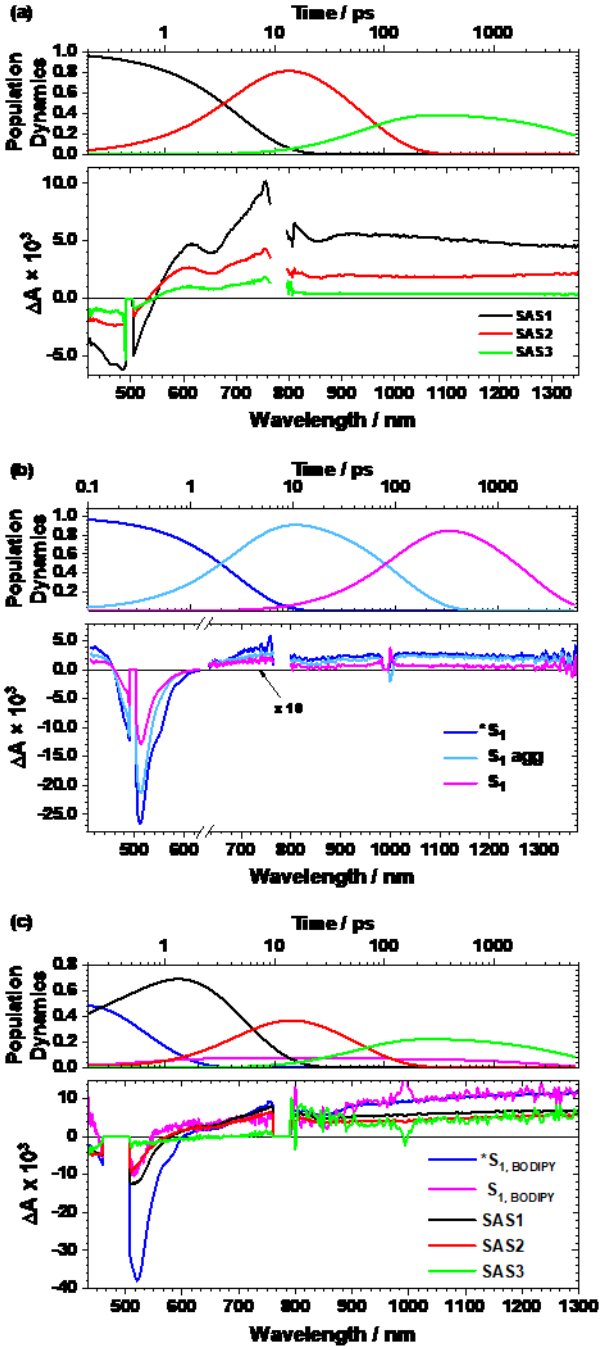

Figure 4. (a) Deconvoluted species-associated spectra (SAS) of GO in water with first species (SAS1, electron-(acoustic) phonon in black), second species (SAS2, shallow de-trapping in red), third species (SAS3, deep de-trapping in green) along with the population dynamics obtained via global-analysis of the data from transient absorption pump-probe studies (λ_{exc} = 500 nm, 600 nJ) using GloTarAn. **(b)** Deconvoluted species-associated spectra (SAS) of PBA-BODIPY in a 97.5:1.25:1.25, H_2O/DMSO/MeOH v/v/v mixture, with first species ($^*S_1$, in blue), second species ($S_{1\ aggregated}$, in light blue), third species (S_1, in magenta) along with the population dynamics obtained via global-analysis of the data from transient absorption pump-probe studies (λ_{exc} = 500 nm, 600 nJ) using GloTarAn. Note: the intensity of the region that

goes from 635 to 1350 nm was multiplied by a factor of 10 for clarity reason. **(c)** Deconvoluted species-associated spectra (SAS) of GO-PBA-BODIPY in water with the first two BODIPY-centred species (SAS1, $^*S_1$(BODIPY) in blue; SAS2, S_1(BODIPY) in magenta), and the three GO-centred species (SAS3, electron-(acoustic) phonon in black; SAS4, shallow de-trapping in red; and SAS5, deep de-trapping in green) along with the population dynamics obtained via global-analysis of the data from transient absorption pump-probe studies (λ_{exc} = 500 nm, 600 nJ) using GloTarAn.

When turning to GO-PBA-BODIPY, the corresponding transient absorption spectra featured contributions from both GO and PBA-BODIPY (Figure 4c). Pumping at 500 nm ensures the photoexcitation of GO as well as PBA-BODIPY as part of GO-PBA-BODIPY and also of the equilibrated free PBA-BODIPY. Therefore, a parallel deactivation model was considered for the global-target analysis (Figure 5). The first species, populated upon photoexcitation, is a hot-$^*S_1$(BODIPY), that is, a vibrationally hot PBA-BODIPY-centred state. This is similar to the corresponding species for the PBA-BODIPY reference. We were unable to resolve contributions from the covalently linked and free PBA-BODIPY. As such, we treated them as a single species. Its underlying state is characterized by a lifetime of less than 1 ps and in our model it deactivates in parallel via two independent branches. On one hand, it is energy transfer toward GO, which accounts for 95% of the deactivation corresponding to GO-PBA-BODIPY. This energy transfer branch includes three additional states with lifetimes of 5.2 ps, 57.4 ps, and 5.29 ns, respectively. These lifetimes and also the differential absorption features are similar to those obtained for the GO reference. The remaining 5%, on the other hand, represents a process in the equilibrated free PBA-BODIPY. It vibrationally relaxes to the S_1(BODIPY) state. The latter is characterized by a lifetime of 2.7 ns and, in turn, is the fluorescent PBA-BODIPY state. This picture is fully consistent with the steady-state spectroscopy measurements, fluorescence quantum yields, and TCSPC lifetimes.

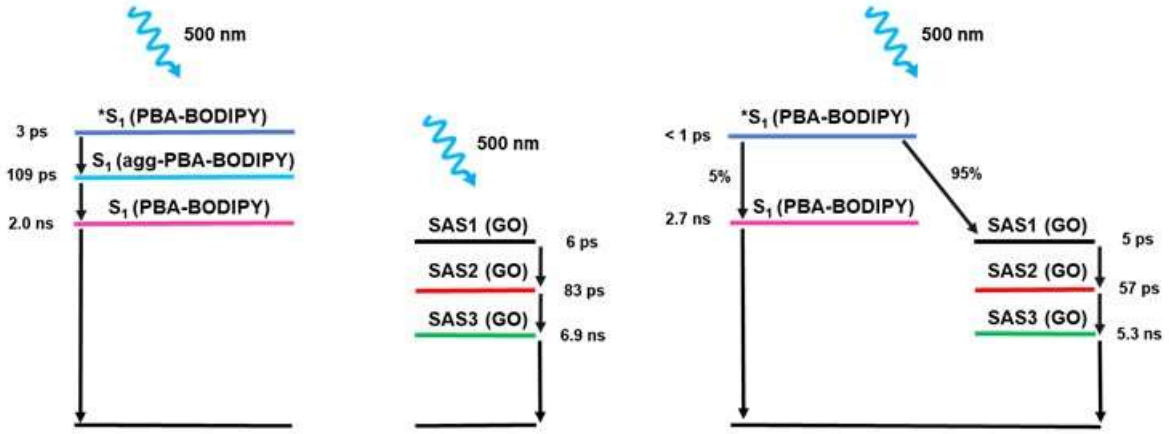

Figure 5. Deactivation model for PBA-BODIPY (left), GO (center), and GO-PBA-BODIPY (right) upon photoexcitation at 500 nm.

For GO-NH-BODIPY, we considered a purely sequential model on the basis of three species. This deemed necessary because no contributions from any BODIPY excited-state transients were noted. As a matter of fact, this is in line with the observations made in the steady-state measurements (Figure S12b). The spectroscopic characteristics are, in general, all very similar and, in particular, similar to those recorded for GO. The lifetimes of each species were 3.4 ps, 43.8 ps, and 4.4 ns. As observed for GO-PBA-BODIPY, the lifetimes, which are associated with the electron de-trapping, are shorter than that seen for pristine GO. After all, GO functionalization seems to be responsible for this difference.

3. Conclusion

The photophysical properties of two different GO-BODIPYs were studied in detail. The utilization of a long but flexible spacer afforded strong electronic GO-BODIPY interactions in the ground state. This drastically altered the light absorption of the BODIPY fragments and impedes the selective BODIPY excitation in GO-NH-BODIPY. In contrast, the use of a short, but rigid spacer based on boronic esters resulted in minor electronic GO-BODIPY interactions in the ground state. Analysis of the excited state interactions in GO-PBA-BODIPY revealed that an ultrafast energy transfer (<1 ps) from PBA-BODIPY to GO is responsible for any of the BODIPY-centred emission quenching. Owing to the dynamic nature of the boronic ester bonds, covalently bound PBA-BODIPY coexists with free PBA-BODIPY in GO-PBA-BODIPY. This results in weak, but nevertheless detectable emission from free PBA-BODIPY, thus, making this strategy potentially affordable for drug delivery due to slow release of BODPY from the GO surface.

Supporting Information

Supporting Information is available from the Wiley Online Library.

Data Availability Statement

The data that support the findings of this study are available from the authors upon request.

Conflict of Interest

The authors declare no conflict of interest.

Acknowledgments

This work was partly supported by the Centre National de la Recherche Scientifique (CNRS) through the International Research Project MULTIDIM between UPR3572 and Okayama University, and by the Interdisciplinary Thematic Institute SysChem via the IdEx Unistra (ANR-10-IDEX-0002) within the program Investissement d'Avenir. C. Ménard-Moyon and B. Richichi thank the Ministries of Europe and Foreign Affairs (MEAE) and of Higher Education and Research (MESR) for their support through the PHC GALILEE 2022 program number 47791TD. The authors wish to thank C. Corcelle and L. Jacquemin for their help for the FTIR measurements.

References

[1] K. S. Novoselov, A. K. Geim, S. v. Morozov, D. Jiang, Y. Zhang, S. v. Dubonos, I. v. Grigorieva, A. A. Firsov, *Science (1979)* **2004**, *306*, 666–669.

[2] A. Razaq, F. Bibi, X. Zheng, R. Papadakis, S. H. M. Jafri, H. Li, *Materials* **2022**, *15*, 1012.

[3] A. M. Pinto, F. D. Magalhães, *Polymers* **2021**, *13*, 685.

[4] J. ; Liu, S. ; Bao, X. Wang, H. Duong Ngo, G. Zhou, N. Luo, J. ; Liu, S. ; Bao, X. Wang, *Micromachines* **2022**, *13*, 184.

[5] S. Zhou, L. Zhang, L. Xie, J. Zeng, B. Qiu, M. Yan, Q. Liang, T. Liu, K. Liang, P. Chen, B. Kong, *Anal Chem* **2021**, *93*, 2982–2987.

[6] S. Roy, N. Soin, R. Bajpai, D. S. Misra, J. A. McLaughlin, S. S. Roy, *J Mater Chem* **2011**, *21*, 14725–14731.

[7] X. Li, Y. Wang, Y. Zhao, J. Zhang, L. Qu, *Small Struct* **2022**, *3*, 2100124.

[8] L. Zhang, S. Zhou, L. Xie, L. Wen, J. Tang, K. Liang, X. Kong, J. Zeng, R. Zhang, J. Liu, B. Qiu, L. Jiang, B. Kong, L. Zhang, S. Zhou, L. Xie, J. Zeng, R. Zhang, J. Liu, B. Qiu, B. Kong, L. Wen, X. Kong, L. Jiang, J. Tang, K. Liang, *Small* **2021**, *17*, 2100141.

[9] G. Reina, J. M. González-Domínguez, A. Criado, E. Vázquez, A. Bianco, M. Prato, *Chem Soc Rev* **2017**, *46*, 4400–4416.

[10] P. Zare, M. Aleemardani, A. M. A. Seifalian, Z. Bagher, A. M. A. Seifalian, *Nanomater* **2021**, *11*, 1083.

[11] S. Guo, S. Garaj, A. Bianco, C. Ménard-Moyon, *Nat Rev Phys* **2022**, *4*, 247–262.

[12] J. Tricomi, M. Cacaci, G. Biagiotti, L. Caselli, L. Niccoli, R. Torelli, A. Gabbani, M. Di Vito, F. Pineider, M. Severi, M. Sanguinetti, E. Menna, M. Lelli, D. Berti, S. Cicchi, F. Bugli, B. Richichi, *Nanoscale* **2022**, *14*, 10190–10199.

[13] G. Biagiotti, A. Salvatore, G. Toniolo, L. Caselli, M. Di Vito, M. Cacaci, L. Contiero, T. Gori, M. Maggini, M. Sanguinetti, D. Berti, F. Bugli, B. Richichi, S. Cicchi, *ACS Appl Mater Interfaces* **2021**, *13*, 26288–26298.

[14] R. Kurapati, C. Martìn, V. Palermo, Y. Nishina, A. Bianco, *Faraday Discuss* **2021**, *227*, 189–203.

[15] M. Orecchioni, V. Bordoni, C. Fuoco, G. Reina, H. Lin, M. Zoccheddu, A. Yilmazer, B. Zavan, G. Cesareni, D. Bedognetti, A. Bianco, L. G. Delogu, M. Orecchioni, V. Bordoni, M. Zoccheddu, L. G. Delogu, C. Fuoco, G. Cesareni, T. V. Rome, G. Reina, H. Lin, A. Bianco, A. Yilmazer, B. Zavan, D. Bedognetti, *Small* **2020**, *16*, 2000123.

[16] S. Y. Wang, C. F. Wang, Y. K. Lv, S. G. Shen, *TrAC Trends Analy Chem* **2018**, *106*, 53–61.

[17] R. Xing, T. Jiao, Y. Liu, K. Ma, Q. Zou, G. Ma, X. Yan, *Polymers* **2016**, *8*, 181.

[18] S. K. Tripathi, R. Goyal, K. C. Gupta, P. Kumar, *Carbon* **2013**, *51*, 224–235.

[19] G. Reina, A. Ruiz, D. Murera, Y. Nishina, A. Bianco, *ACS Appl Mater Interfaces* **2019**, *11*, 7695–7702.

[20] R. Rauti, M. Medelin, L. Newman, S. Vranic, G. Reina, A. Bianco, M. Prato, K. Kostarelos, L. Ballerini, *Nano Lett* **2019**, *19*, 2858–2870.

[21] M. L. Agazzi, M. B. Ballatore, A. M. Durantini, E. N. Durantini, A. C. Tomé, *Journal of Photochemistry and Photobiology C: Photochemistry Reviews* **2019**, *40*, 21–48.

[22] E. Antina, N. Bumagina, Y. Marfin, G. Guseva, L. Nikitina, D. Sbytov, F. Telegin, *Molecules 2022, Vol. 27, Page 1396* **2022**, *27*, 1396.

[23] L. Wang, Z. Xiong, X. Ran, H. Tang, D. Cao, *Dyes and Pigments* **2022**, *198*, 110040.

[24] J. L. Wang, L. Zhang, M. J. Zhao, T. Zhang, Y. Liu, F. L. Jiang, *ACS Appl Bio Mater* **2021**, *4*, 1760–1770.

[25] Y. Liu, C. Xu, L. Teng, H. W. Liu, T. B. Ren, S. Xu, X. Lou, H. Guo, L. Yuan, X. B. Zhang, *Chemical Communications* **2020**, *56*, 1956–1959.

[26] Z. Shi, X. Han, W. Hu, H. Bai, B. Peng, L. Ji, Q. Fan, L. Li, W. Huang, *Chem Soc Rev* **2020**, *49*, 7533–7567.

[27] Khoerunnisa, E. B. Kang, Z. A. I. Mazrad, G. Lee, I. In, S. Y. Park, **n.d.**, *71*, 1064–1071.

[28] Y. Su, N. Wang, B. Liu, Y. Du, R. Li, Y. Meng, Y. Feng, Z. Shan, S. Meng, *Dyes and Pigments* **2020**, *177*, 108262.

[29] E. de la O-Cuevas, V. Alvarez-Venicio, I. Badillo-Ramírez, S. R. Islas, M. del P. Carreón-Castro, J. M. Saniger, *Spectrochim Acta A Mol Biomol Spectrosc* **2021**, *246*, 119020.

[30] G. Reina, A. Ruiz, B. Richichi, G. Biagiotti, G. E. Giacomazzo, L. Jacquemin, Y. Nishina, C. Ménard-Moyon, W. T. Al-Jamal, A. Bianco, *2d Mater* **2022**, *9*, 015038.

[31] N. D. Q. Chau, G. Reina, J. Raya, I. A. Vacchi, C. Ménard-Moyon, Y. Nishina, A. Bianco, *Carbon N Y* **2017**, *122*, 643–652.

[32] I. A. Vacchi, C. Spinato, J. Raya, A. Bianco, C. Ménard-Moyon, *Nanoscale* **2016**, *8*, 13714–13721.

[33] G. Reina, C. Gabellini, M. Maranska, F. Grote, S. M. Chin, L. Jacquemin, F. Berger, P. Posocco, S. Eigler, A. Bianco, *Carbon N Y* **2022**, *195*, 69–79.

[34] A. G. Shard, *Surface and Interface Analysis* **2014**, *46*, 175–185.

[35] K. A. Wepasnick, B. A. Smith, J. L. Bitter, D. Howard Fairbrother, *Anal Bioanal Chem* **2010**, *396*, 1003–1014.

[36] Z. Luo, Y. Lu, L. A. Somers, A. T. C. Johnson, *J Am Chem Soc* **2009**, *131*, 898–899.

[37] G. E. Giacomazzo, P. Palladino, C. Gellini, G. Salerno, V. Baldoneschi, A. Feis, S. Scarano, M. Minunni, B. Richichi, *RSC Adv* **2019**, *9*, 30773–30777.

[38] T. T. Tran, T. C. Vu, H. van Hoang, W. F. Huang, H. T. Pham, H. M. T. Nguyen, *ACS Omega* **2022**, *7*, 37221–37228.

[39] F. Mouhat, F. X. Coudert, M. L. Bocquet, *Nat Commun* **2020**, *11*, 1566.

[40] M. A. Martínez-Aguirre, D. M. Otero, M. L. Álvarez-Hernández, T. Torres-Blancas, A. Dorazco-González, A. K. Yatsimirsky, *Heterocycl Comm* **2017**, *23*, 171–180.

[41] K. P. Loh, Q. Bao, G. Eda, M. Chhowalla, **2010**, *2*, 1015–1024.

[42] F. Lu, H. Zhang, W. Pan, N. Li, B. Tang, *Chemical Communications* **2021**, *57*, 7067–7082.

[43] X. Wu, Z. Li, X. X. Chen, J. S. Fossey, T. D. James, Y. B. Jiang, *Chem Soc Rev* **2013**, *42*, 8032–8048.

[44] J. J. Cash, T. Kubo, A. P. Bapat, B. S. Sumerlin, *Macromolecules* **2015**, *48*, 2098–2106.

[45] A. Naumov, F. Grote, M. Overgaard, A. Roth, C. E. Halbig, K. Nørgaard, D. M. Guldi, S. Eigler, *J Am Chem Soc* **2016**, *138*, 11445–11448.

[46] L. Wang, H. Y. Wang, Y. Wang, S. J. Zhu, Y. L. Zhang, J. H. Zhang, Q. D. Chen, W. Han, H. L. Xu, B. Yang, H. B. Sun, *Advanced Materials* **2013**, *25*, 6539–6545.

[47] S. Kumar, M. Anija, N. Kamaraju, K. S. Vasu, K. S. Subrahmanyam, A. K. Sood, C. N. R. Rao, *Appl Phys Lett* **2009**, *95*, 191911.

[48] Q. Zhang, H. Zheng, Z. Geng, S. Jiang, J. Ge, K. Fan, S. Duan, Y. Chen, X. Wang, Y. Luo, *J Am Chem Soc* **2013**, *135*, 12468–12474.

[49] S. Kaniyankandy, S. N. Achary, S. Rawalekar, H. N. Ghosh, *Journal of Physical Chemistry C* **2011**, *115*, 19110–19116.

[50] E. Carpene, E. Mancini, C. Dallera, D. Schwert, C. Ronning, S. De Silvestrl, *New J Phys* **2007**, *9*, 404.